Suppressing Void Formation in All-Solid-State Batteries: The Role of Interfacial Adhesion on Alkali Metal Vacancy Transport

Ieuan David Seymour* and Ainara Aguadero

Supplementary Methods

Model Surface Selection

For BCC Li and Na metal, only the (100) surface was studied as it was previously shown to be the lowest energy surface from DFT calculations.[1] For HCP Li metal, the $(10\bar{1}0)$ and (0001) surfaces were studied. The stoichiometric (100) surface was previously found to be a low energy surface termination for the cubic alkali halide phases LiCl, NaCl and NaBr.[2] In addition to being simple ionic solids, the alkali halides have also been proposed to be formed during the decomposition reaction of several state-of-the-art electrolyte materials such as Li_6PS_5Cl[3] and Li_3InCl_6[4] with $Na_3Y_{1-x}Zr_xCl_6$[5], with alkali metals. Li_3OCl is a promising transition metal free solid electrolyte material that is stable against Li metal.[6] The (100) surface was also found to be a low energy for cubic Li_3OCl with two possible non-stoichiometric terminations: Cl terminated and O terminated, which were both studied in this work.[7] The Cl and O terminated surface contain additional formula units of LiCl and Li_2O, respectively, and so the excess chemical potential in eqn (1) in the main text was referenced to the LiCl and Li_2O unit cell energies.

LiMg and AlSc were chosen as metallic alloy compounds to model the interface of BCC Li metal with metallic interlayer or current collector materials. The B2 CsCl phase of AlSc adopts an ordered BCC structure with very similar lattice parameters to Li metal.[8] Li-Mg alloys form a solid solution with a BCC structure up to approximately 70 at% Mg.[9] A previous DFT study indicated that an ordered B2 phase of LiMg is expected at low temperature.[10] The B2 LiMg phase also has a similar lattice parameter to BCC Li metal and from DFT energies taken from the Materials Project, the reaction of 2Li + LiMg → Li_3Mg is predicted to have a small reaction energy of 0.004 eV/atom.[11] To the best of our knowledge, the energies of different surface terminations of LiMg and AlSc have not been previously studied. In this study we chose the (100) surface for comparison with the halide systems. The (100) termination also leads to non-stoichiometric surfaces for both LiMg (Li-terminated and Mg-terminated) and AlSc (Al-terminated and Sc-terminated). For LiMg, only the Mg terminated surface was studied. The excess chemical potential of Mg was calculated from the unit cell energy of Mg ($Fm\bar{3}m$) metal. For AlSc, both the Al- and Sc-terminated surfaces were studied. The excess chemical potential was referenced from unit cell structures of Al ($Fm\bar{3}m$) and Sc ($P6_3/mmc$) metal.

Li_2O was chosen as a stable oxide of lithium metal that rapidly forms when Li metal comes into contact with O_2.[12] In addition to being a predicted decomposition product for many oxide solid electrolyte materials with Li metal,[13] it is also an important component of the inner layer of the solid electrolyte interface (SEI) in liquid electrolyte batteries containing Li metal anodes.[14] Li_2O adopts a cubic structure in which the stoichiometric (111) plane has previously been predicted to be lowest energy facet.[15] γ-Li_3PO_4 was selected as a model phosphate electrolyte that is the end member composition of the $Li_xPO_yN_z$ (LiPON)[16] and γ-$Li_{3+x}P_{1-x}Si_xO_4$[17] family of materials. The addition of a thin γ-Li_3PO_4 layer has also been shown to improve the interfacial adhesion in the Li/$Li_7La_3Zr_2O_{12}$ system.[18] The interface of Li metal and γ-Li_3PO_4 has also previously been studied in a number of computational works.[19,20] In contact with Li metal, γ-Li_3PO_4 is predicted from the Materials Project to decompose through the reaction Li_3PO_4+8 Li → 4Li_2O+Li_3P, with a reaction energy of 0.344 eV/atom.[11] γ-Li_3PO_4 therefore serves as an interesting test system which is thermodynamically unstable against Li, but may show a degree of kinetic stability as a result of the structural rearrangement required to form the Li_2O and Li_3P secondary phases. γ-Li_3PO_4 adopts an orthorhombic structure in which the (100) surface has the lowest energy.[21]

Li_2S and Li_3P were chosen as common decomposition products that form when solid electrolyte materials such as argyrodite, Li_6PS_5Cl, are put into contact with lithium metal. Li_2S adopts a cubic $Fm\bar{3}m$ structure, analogous to Li_2O. The stoichiometric (111) surface was previously found to be a low energy surface for Li_2S.[22] Due to the large lattice parameter of the DFT optimised Li_2S unit cell (5.711Å), a coherent interface with the low energy surfaces of BCC or HCP Li could not be formed. An incoherent interface was therefore constructed between the stoichiometric Li_2S (111) surface and the BCC Li (100) surface to study the average work of adhesion. Coincident site lattice (CSL) theory in the MPinterfaces code[23] was used to find a supercell with minimal lattice mismatch between Li (100) and Li_2S (111). The relationship between the lattice parameters in the *ab* plane of the interface supercell (sup) and initial

conventional BCC Li and primitive Li_2S unit cells were $a_{sup,Li}=2a_{BCC,Li}$, $b_{sup,Li}=3\ b_{BCC,Li}+a_{BCC,Li}$ and $a_{sup,Li2S}=2a_{Li2S}- b_{Li2S}$, $b_{sup,Li2S}=2b_{Li2S}+a_{Li2S}$, respectively. Li_3P adopts a hexagonal $P6_3/mmc$ structure.[24] The stoichiometric (001) surface has previously been studied as low energy facet of the Li_3P structure.[25] To further confirm this, all distinct stoichiometric surfaces of the primitive Li_3P $P6_3/mmc$ unit cell were considered up to a *hkl* index of 2, and the (001) surface was found to be the lowest surface with a surface energy of 0.485 J/m^2. As was the case for Li_2S, a coherent interface with the Li_3P (001) surface and Li metal could not be formed and so an incoherent CSL interface between the BCC Li (100) and Li_3P (001) surfaces was constructed. The relationship between the lattice parameters in the *ab* plane of the interface supercell (sup) and initial conventional BCC Li and conventional Li_3P unit cells were $a_{sup,Li}=3a_{BCC,Li}-b_{BCC,Li}$, $b_{sup,Li}=3\ b_{BCC,Li}+6a_{BCC,Li}$ and $a_{sup,Li3P}=3a_{Li3P}- 1_{Li3P}$, $b_{sup,Li3P}=6b_{Li3P}+3a_{Li3P}$, respectively.

Supplementary Figures

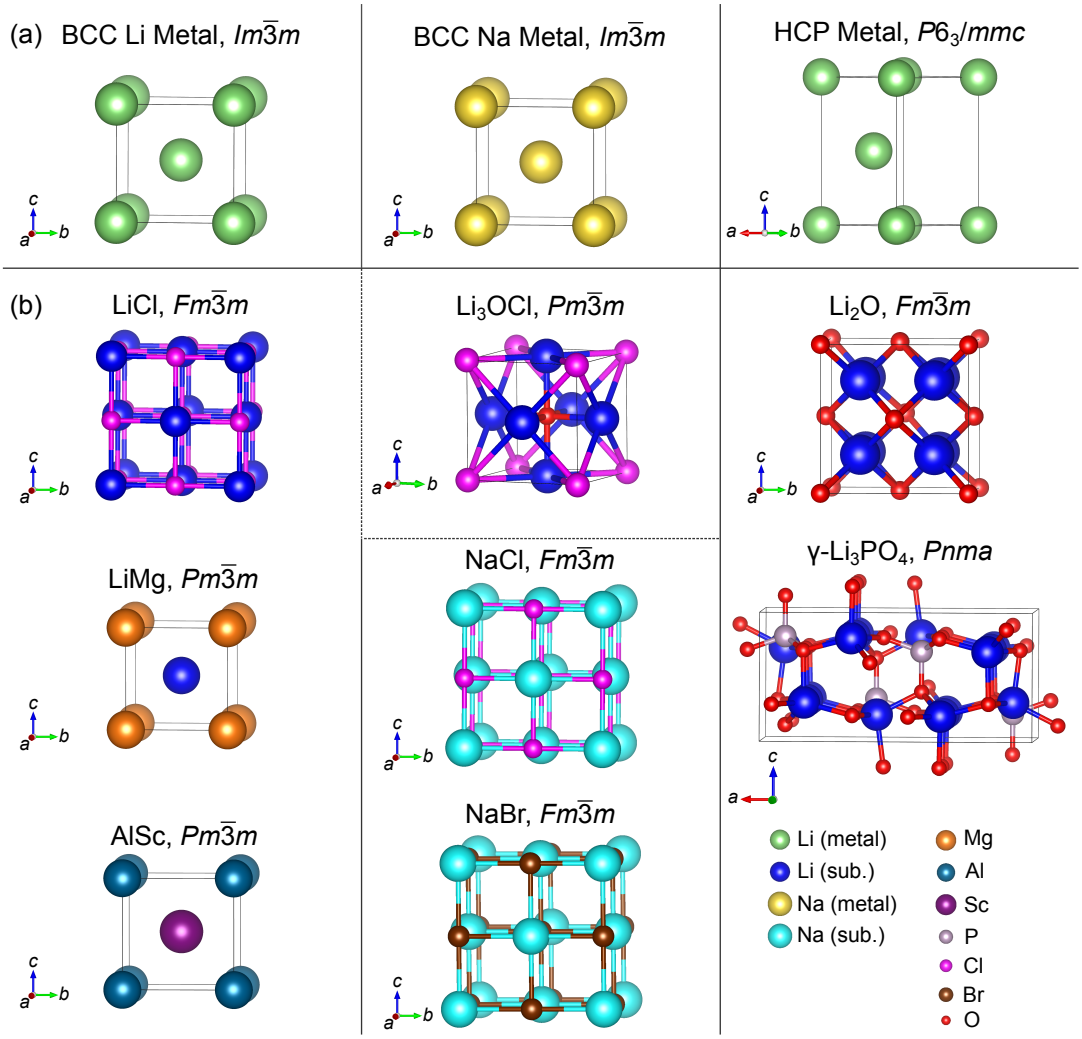

Fig. S1: Unit cell structures of (a) body centred cubic (BCC) and hexagonal close packed (HCP) alkali metals, Li and Na and (b) substrate phases. Different colouring is used for the Li/Na atoms in the alkali metal unit cells and substrate phases to distinguish them. Vertical lines indicate which combinations of alkali metal unit cells and substrate materials were studied as interface models. The Li_3OCl structure was studied with both BCC Li and Na.

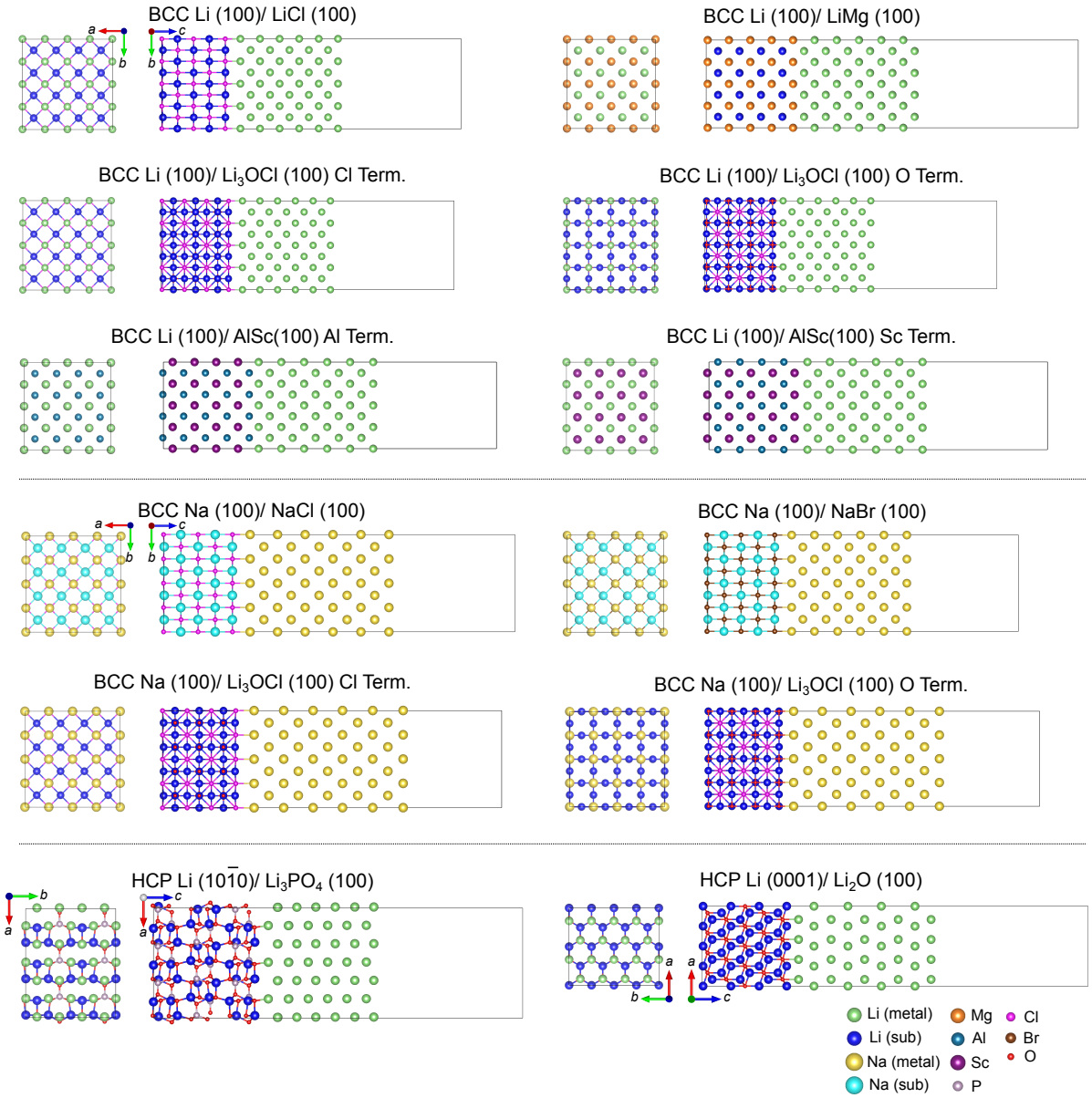

Fig. S2: DFT relaxed alkali metal/solid-state electrolyte interface structures. For all structures, a strain was applied to the body centred cubic (BCC) or hexagonal close packed (HCP) alkali metal (Li or Na) slab to match the lattice parameters of the substrate phase. Different colouring is used for the Li/Na atoms in the alkali metal unit cells and substrate phases to distinguish them.

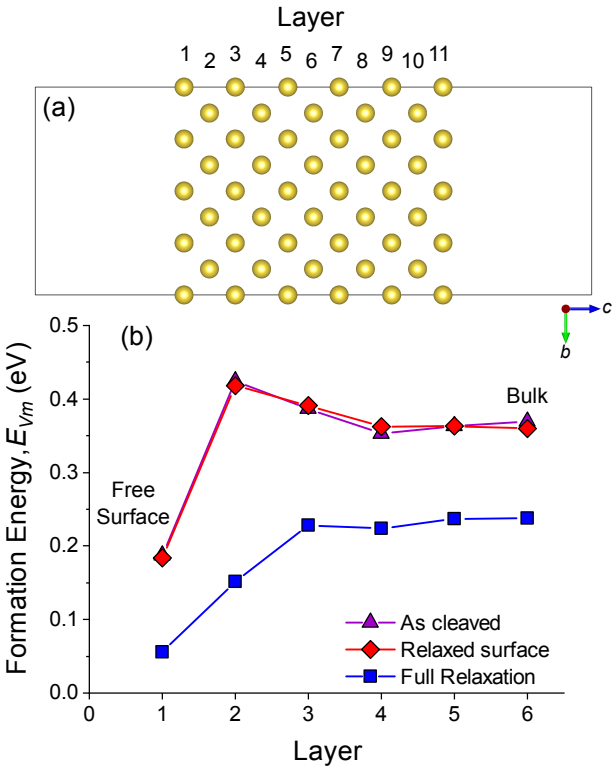

Fig. S3: (a) BCC Na (100) slab structure containing 11 Li layers. (b) Variation in Na-vacancy formation energy, E_{Vm}, in different layers from the slab surface (layer 1) to the slab bulk (layer 6). Vacancy formation energies were calculated for Na slabs without relaxation (as-cleaved), with surface relaxation (relaxed surface) and with full relaxation of all atoms.

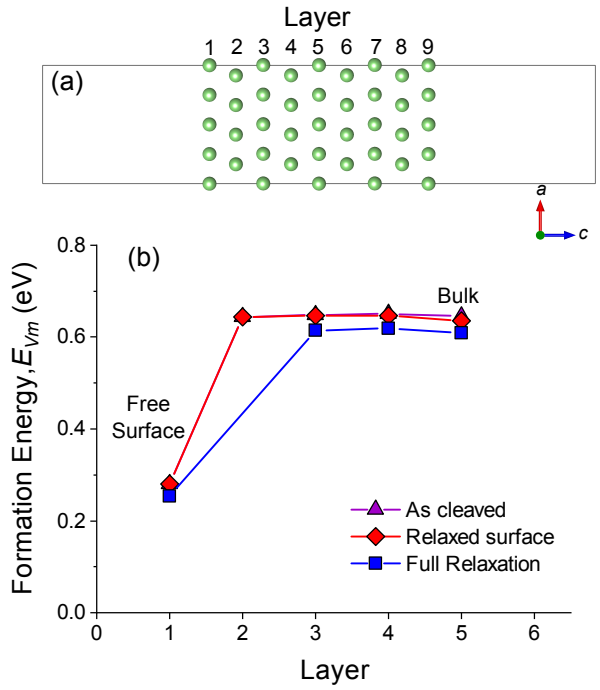

Fig. S4: (a) HCP Li (0001) slab structure containing 9 Li layers. (b) Variation in Li-vacancy formation energy, E_{Vm}, in different layers from the slab surface (layer 1) to the slab bulk (layer 5). Vacancy formation energies were calculated for Li slabs without relaxation (as-cleaved), with surface relaxation (relaxed surface) and with full relaxation of all atoms. After full relaxation, the Li vacancy in layer 2 spontaneously migrated to layer 1.

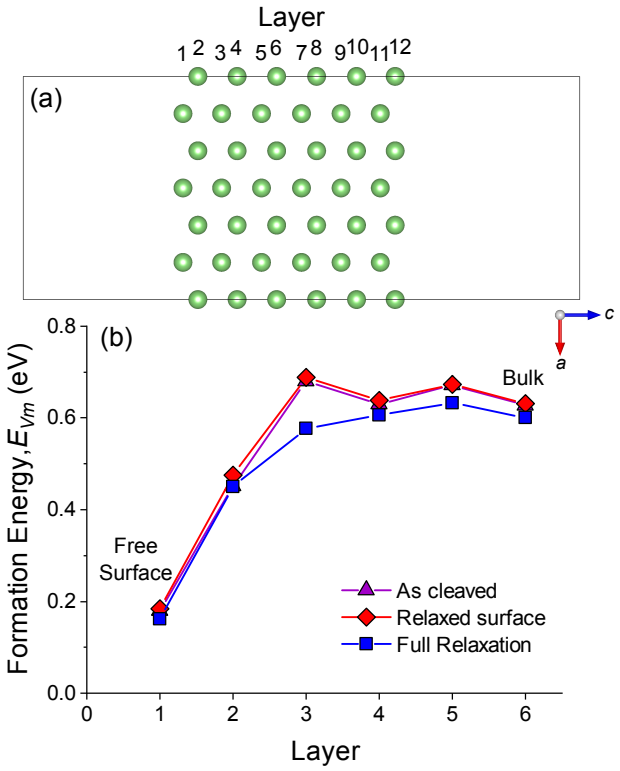

Fig. S5: (a) HCP Li $(10\bar{1}0)$ slab structure containing 12 Li layers. (b) Variation in Li-vacancy formation energy, E_{Vm}, in different layers from the slab surface (layer 1) to the slab bulk (layer 6). Vacancy formation energies were calculated for Li slabs without relaxation (as-cleaved), with surface relaxation (relaxed surface) and with full relaxation of all atoms.

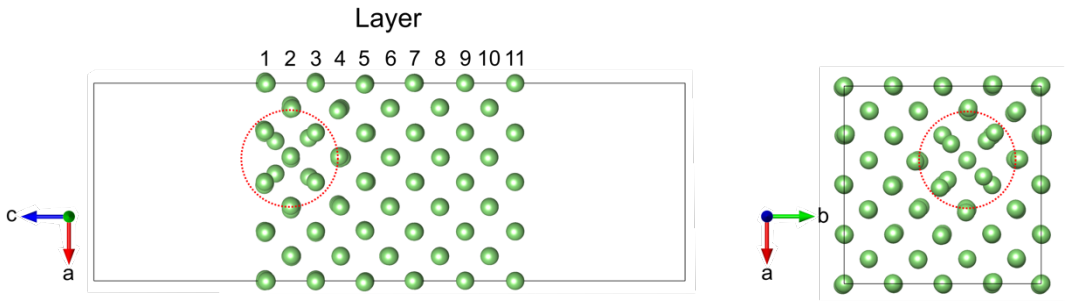

Fig. S6: BCC Li (100) slab structure with a Li vacancy in layer 2 relative to the surface (layer 1). The large relation of the neighbouring Li atoms around the vacant site is indicated with the red dashed circle.

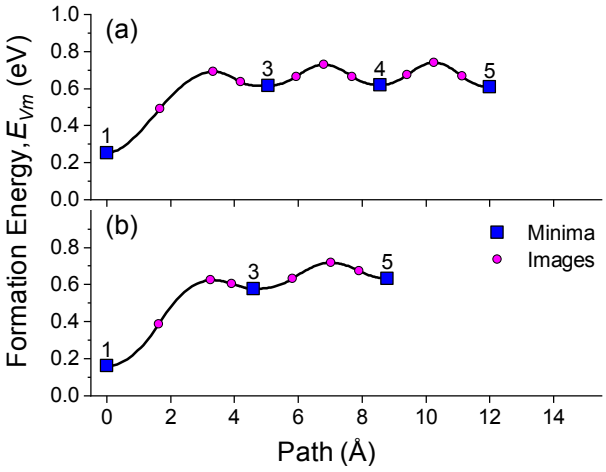

Fig. S7: Nudged elastic band activation barriers for Li vacancy diffusion between the surface and bulk of (a) (0001) and (b) $(10\bar{1}0)$ terminated slabs of HCP Li. Labels above the local minima (blue squares) indicate the layer number in the supercell.

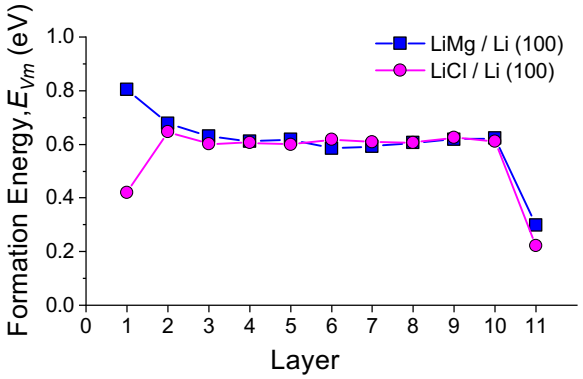

Fig. S8: Comparison of Li vacancy formation energy, E_{Vm} , in BCC Li without vacancy relaxation in different layers away from the Li surface (layer 1) of a LiMg (100)/Li (100) and LiCl (100)/Li (100) interface. Strains of -0.14 and +5.67%, respectively, were applied to the Li slab lattice parameters within the interfacial plane.

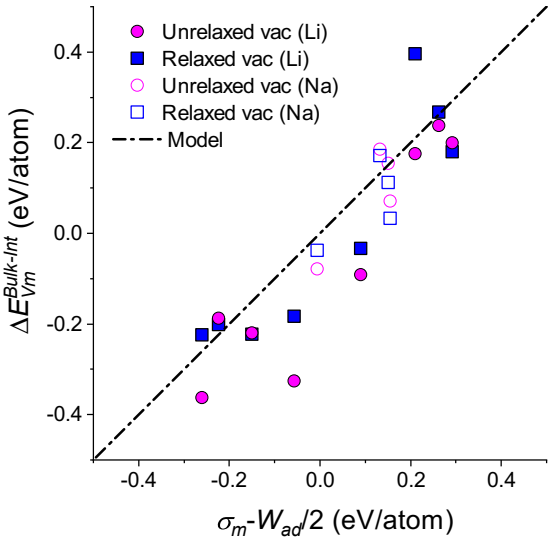

Fig. S9: Plot of vacancy segregation energy ($\Delta E_{Vm}^{Bulk-Int}$) with surface energy σ_m and work of adhesion W_{ad}, for coherent alkali metal/substrate interface. The bond breaking model from eqn (11) in the main text is shown as a dot-dash line. Li and Na metals systems are shown with closed and open symbols For all structures, $\Delta E_{Vm}^{Bulk-Int}$ is calculated with (squares) and without (circles) relaxation around the vacancies.

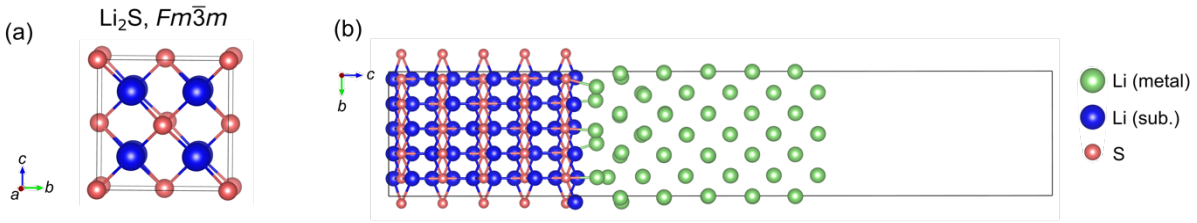

Fig. S10: (a) Unit cell structure of Li_2S ($Fm\bar{3}m$). (b) DFT relaxed BCC Li (100)/Li_2S (111) incoherent interface structure containing 11 Li metal layers. A strain of -1.7% and +1.7% was applied to the *a* and *b* lattice parameters, respectively, of the body centred cubic (BCC) Li slab to match the Li_2S substrate. Different colouring is used for the Li/Na atoms in the alkali metal unit cells and substrate phases to distinguish them. Significant relaxation of the Li metal atoms occurred at the BCC Li (100)/Li_2S (111) boundary (layer 1), due to the incoherent nature of the interface.

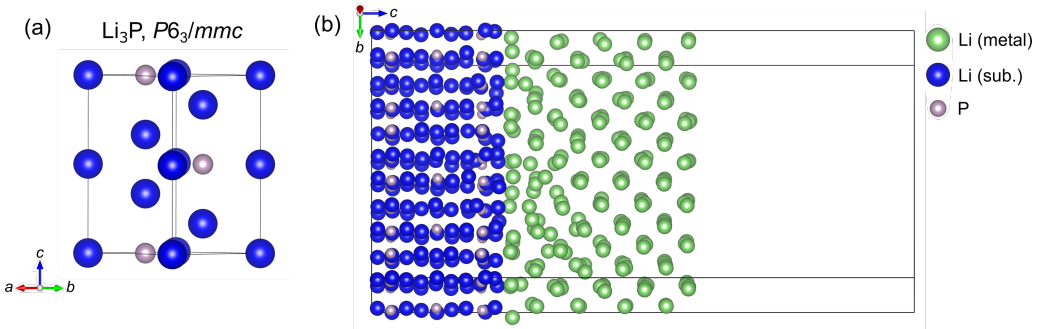

Fig. S11: Unit cell structure of Li_3P $P6_3/mmc$. (b) DFT relaxed BCC Li (100)/Li_3P (001) incoherent interface structure containing 9 Li metal layers. A strain of –3.0% and +2.8% was applied to the *a* and *b* lattice parameters, respectively, of the body centred cubic (BCC) Li slab to match the Li_3P substrate. Different colouring is used for the Li/Na atoms in the alkali metal unit cells and substrate phases to distinguish them. Significant relaxation of the Li metal atoms occurred at the BCC Li (100)/Li_3P (001) boundary (layer 1), due to the incoherent nature of the interface.

Supplementary Tables

Table S1: DFT optimised lattice parameters for body centred cubic (BCC) and hexagonal close packed (HCP) structures of Li and Na metal.

Alkali metal	Structure	Lattice Parameter (Å)	
		a	*c*
Li	BCC	3.436	-
	HCP	3.068	4.979
Na	BCC	4.194	-

Table S2: DFT optimised lattice parameters for cubic substrate phases paired with the BCC Li (100) surface. The transformation and strain applied to the BCC Li lattice to maintain coherency with the substrate is shown for each structure.

Substrate	Substrate lattice parameter, a_{sub} (Å)	Alkali Metal Surface	Substrate Surface	Interface Transformation	Strained lattice Parameter, $a_{Li,BCC}$ (Å)	Strain (%) $a_{Li,BCC}$
LiCl	5.152	(100)	(100)	$a_{Li,BCC} = (\sqrt{2}/2)a_{sub}$	3.643	5.67
LiMg	3.432	(100)	(100)	$a_{Li,BCC} = a_{sub}$	3.432	-0.14
AlSc	3.372	(100)	(100)	$a_{Li,BCC} = a_{sub}$	3.372	-1.90
Li_3OCl	3.886	(100)	(100)	$a_{Li,BCC} = a_{sub}$	3.886	11.58

Table S3: DFT optimised lattice parameters for cubic substrate phases paired with the BCC Na (100) surface. The transformation and strain applied to the BCC Na lattice to maintain coherency with the substrate is shown for each structure.

Substrate	Substrate lattice parameter, a_{sub} (Å)	Alkali Metal Surface	Substrate Surface	Interface Transformation	Strained lattice Parameter, $a_{Na,BCC}$ (Å)	Strain (%) $a_{Na,BCC}$
NaCl	5.650	(100)	(100)	$a_{Na,BCC} = (\sqrt{2}/2)a_{sub}$	3.995	-4.97
NaBr	6.028	(100)	(100)	$a_{Na,BCC} = (\sqrt{2}/2)a_{sub}$	4.262	1.60
Li_3OCl	3.886	(100)	(100)	$a_{Na,BCC} = a_{sub}$	3.886	-7.92

Table S4: DFT optimised lattice parameters for substrate phases paired with the HCP Li (0001) and $(10\bar{1}0)$ surfaces. The transformation and strain applied to the HCP lattice to maintain coherency with the substrate is shown for each structure.

Substrate	Substrate lattice parameter (Å)			Alkali Metal Surface	Substrate Surface	Interface Transformation	Strained lattice Parameter, $a_{Na,BCC}$ (Å)		Strain (%)	
	a_{sub}	b_{sub}	c_{sub}				$a_{Li,HCP}$	$c_{Li,HCP}$	$a_{Li,HCP}$	$c_{Li,HCP}$
Li_2O	4.633	-	-	(0001)	(111)	$a_{Li,HCP} = (\sqrt{2}/2)a_{sub}$	3.276	-	6.33	
γ-Li_3PO_4	10.570	6.150	4.988	$(10\bar{1}0)$	(100)	$a_{Li,HCP} = b_{sub}/2$, $c_{Li,\mathrm{HCP}} = c_{sub}$	3.075	4.988	0.22	0.19

Table S5: DFT calculated surface energies, σ_m, for different surface facets of Li and Na slabs with body centred cubic (BCC) and hexagonal close packed (HCP) structures. Surface energies were calculated before (as cleaved) and after (relaxed) surface relaxation. Surface planes are given in *hkl* and *hkil* notation for the BCC and HCP systems, respectively. The first nearest neighbour coordination of the surface atoms is given in addition to the surface atom density, ρ. Bulk BCC and HCP have a 1nn coordination of 8 and 12 respectively. For the $(10\bar{1}0)$ HCP Li surface, atoms in the first and second layers were considered as surface.

Metal	Structure	Surface	Slab Layers	ρ (atoms/nm^2)	1nn surf. coord.	Surface energy, σ_m			
						As cleaved		Relaxed	
						(J/m^2)	(eV/atom)	(J/m^2)	(eV/atom)
Li	HCP	(0001)	9	12.26	9	0.604	0.300	0.583	0.290
		$(10\bar{1}0)$	12	13.09	8, 10	0.506	0.258	0.498	0.253
	BCC	(100)	11	8.47	4	0.466	0.343	0.463	0.341
Na	BCC	(100)	11	5.69	4	0.231	0.253	0.230	0.253

Table S6: DFT calculated values of the work of adhesion (W_{ad}), alkali metal surface energy, σ_m, substrate surface energy σ_{sub}, Young-Dupré contact angle, θ and alkali metal vacancy segregation energy $\Delta E_{Vm}^{Bulk-Int}$ for different alkali metal/substrate interfaces.

Alkali metal	Alkali metal structure	Alkali metal surface	Substrate surface	Substrate	σ_m		σ_{sub}	W_{ad}		θ	$\Delta E_{Vm}^{Bulk-Int}$ (eV)		$(\sigma_m - W_{ad}/2)/\rho$
					(eV/atom)	(J/m^2)	(J/m^2)	(eV/atom)	(J/m^2)	(°)	Unrelaxed vac.	Relaxed vac.	(eV/atom)
Li	BCC	(100)	(100)	LiCl (Cl top)	0.391	0.472	0.126	0.199	0.240	119.5	0.198	0.180	0.292
				Li_3OCl (Cl term)	0.395	0.419	0.157	0.264	0.281	109.3	0.238	0.266	0.263
				Li_3OCl (O term)	0.395	0.419	0.726	0.903	0.958	0.0	-0.327	-0.183	-0.057
				AlSc (Al term)	0.322	0.453	1.109	1.164	1.641	0.0	-0.364	-0.224	-0.260
				AlSc (Sc term)	0.322	0.453	1.240	1.091	1.537	0.0	-0.188	-0.202	-0.224
				LiMg (Mg term)	0.340	0.462	0.751	0.978	1.330	0.0	-0.220	-0.223	-0.149
	HCP	(0001)	(111)	Li_2O	0.308	0.531	0.533	0.195	0.337	111.4	0.175	0.346	0.210
		$(10\bar{1}0)$	(100)	γ-Li_3PO_4	0.247	0.515	0.498	0.313	0.654	74.4	-0.091	-0.033	0.090
Na	BCC	(100)	(100)	NaCl	0.226	0.226	0.151	0.150	0.150	109.7	0.154	0.111	0.151
				NaBr	0.243	0.214	0.125	0.174	0.153	106.5	0.070	0.033	0.156
				Li_3OCl (Cl term)	0.188	0.199	0.157	0.111	0.118	114.1	0.185	0.160	0.132
				Li_3OCl (O term)	0.188	0.199	0.726	0.388	0.412	0.0	-0.078	-0.031	-0.006

Table S7: DFT calculated values of the average work of adhesion (W_{ad}), alkali metal surface energy, σ_m, substrate surface energy, σ_{sub}, and Young-Dupré contact angle, θ, for BCC Li (100)/Li_2S (111) and BCC Li (100)/Li_3P (001) incoherent supercell interfaces.

Alkali metal	Alkali metal structure	Alkali metal surface	Substrate surface	Substrate	σ_m		σ_{sub}	Average W_{ad}		θ	$(\sigma_m - W_{ad}/2)/\rho$
					(eV/atom)	(J/m^2)	(J/m^2)	(eV/atom)	(J/m^2)	(°)	(eV/atom)
Li	BCC	(100)	(111)	Li_2S	0.332	0.451	0.333	0.266	0.361	101.5	0.199
			(001)	Li_3P	0.331	0.448	0.485	0.435	0.589	71.1	0.113

References

1 K. S. Nagy, S. Kazemiabnavi, K. Thornton and D. J. Siegel, *ACS Appl. Mater. Interfaces*, 2019, **11**, 7954–7964.
2 P. W. Tasker, *Philos. Mag. A Phys. Condens. Matter, Struct. Defects Mech. Prop.*, 1979, **39**, 119–136.
3 S. Wenzel, S. J. Sedlmaier, C. Dietrich, W. G. Zeier and J. Janek, *Solid State Ionics*, 2018, **318**, 102–112.
4 L. M. Riegger, R. Schlem, J. Sann, W. G. Zeier and J. Janek, *Angew. Chemie*, 2021, **133**, 6792–6797.
5 E. A. Wu, S. Banerjee, H. Tang, P. M. Richardson, J. M. Doux, J. Qi, Z. Zhu, A. Grenier, Y. Li, E. Zhao, G. Deysher, E. Sebti, H. Nguyen, R. Stephens, G. Verbist, K. W. Chapman, R. J. Clément, A. Banerjee, Y. S. Meng and S. P. Ong, *Nat. Commun.*, 2021, **12**, 1–11.
6 Y. Zhao and L. L. Daemen, *J. Am. Chem. Soc.*, 2012, **134**, 15042–15047.
7 K. Kim and D. J. Siegel, *ACS Appl. Mater. Interfaces*, 2019, **11**, 39940–39950.
8 O. Schob and E. Parthé, *Acta Crystallogr.*, 1965, **19**, 214–224.
9 J. A. Catterall, *Nature*, 1952, 169, 336.
10 R. H. Taylor, S. Curtarolo and G. L. W. Hart, *Phys. Rev. B - Condens. Matter Mater. Phys.*, 2010, **81**, 024112.
11 A. Jain, S. P. Ong, G. Hautier, W. Chen, W. D. Richards, S. Dacek, S. Cholia, D. Gunter, D. Skinner, G. Ceder and K. A. Persson, *APL Mater.*, 2013, 1.
12 R. Guo and B. M. Gallant, *Chem. Mater.*, 2020, **32**, 5525–5533.
13 W. D. Richards, L. J. Miara, Y. Wang, J. C. Kim and G. Ceder, *Chem. Mater.*, 2016, **28**, 266–273.
14 A. Schechter, D. Aurbach and H. Cohen, *Langmuir*, 1999, **15**, 3334–3342.
15 M. D. Radin, J. F. Rodriguez, F. Tian and D. J. Siegel, *J. Am. Chem. Soc.*, 2012, **134**, 1093–1103.
16 J. B. Bates, N. J. Dudney, G. R. Gruzalski, R. A. Zuhr, A. Choudhury, C. F. Luck and J. D. Robertson, *Solid State Ionics*, 1992, **53**–**56**, 647–654.
17 A. Khorassani, G. Izquierdo and A. R. West, *Mater. Res. Bull.*, 1981, **16**, 1561–1567.
18 Y. Ruan, Y. Lu, X. Huang, J. Su, C. Sun, J. Jin and Z. Wen, *J. Mater. Chem. A*, 2019, **7**, 14565–14574.
19 K. C. Santosh, K. Xiong, R. C. Longo and K. Cho, *J. Power Sources*, 2013, **244**, 136–142.
20 N. D. Lepley and N. A. W. Holzwarth, *Phys. Rev. B - Condens. Matter Mater. Phys.*, 2015, **92**, 214201.
21 N. D. Lepley, N. A. W. Holzwarth and Y. A. Du, *Phys. Rev. B - Condens. Matter Mater. Phys.*, 2013, **88**, 104103.
22 Z. Liu, D. Hubble, P. B. Balbuena and P. P. Mukherjee, *Phys. Chem. Chem. Phys.*, 2015, **17**, 9032–9039.
23 K. Mathew, A. K. Singh, J. J. Gabriel, K. Choudhary, S. B. Sinnott, A. V. Davydov, F. Tavazza and R. G. Hennig, *Comput. Mater. Sci.*, 2016, **122**, 183–190.
24 Y. Dong and F. J. Disalvo, *Acta Crystallogr. Sect. E Struct. Reports Online*, 2007, **63**, i97–i98.
25 Y. Kim, D. Koo, S. Ha, S. C. Jung, T. Yim, H. Kim, S. K. Oh, D. M. Kim, A. Choi, Y. Kang, K. H. Ryu, M. Jang, Y. K. Han, S. M. Oh and K. T. Lee, *ACS Nano*, 2018, **12**, 4419–4430.